ACS Catalysis

pubs.acs.org/acscatalysis Research Article

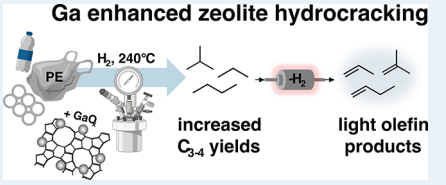
Gallium-Containing ZSM-5 Zeolites Improve Hydrocracking Selectivity to Propane

Anna E. Brenner, Faisal H. Alshafei, Juliana Lu-Yang, Ozge D. Bozkurt, Marcos G. Farpón, Colum O'Leary, Arun Asundi, Bowei Liu, Rachita Rana, Griffin Drake, Simon R. Bare, Gregg T. Beckham, and Yuriy Román-Leshkov*

Cite This: https://doi.org/10.1021/acscatal.6c06722 Read Online

ACCESS | Metrics & More | Article Recommendations | Supporting Information

ABSTRACT: Polyolefin hydrocracking over Brønsted acidic ZSM-5 produces light hydrocarbons with narrow product distributions, but further increases in propane and butane selectivity are required to improve process economics and sustainability. Here, we examined the effect of various metal and metal oxide dopants, namely Pt, Pt-Sn, SnO_x, ZnO_x, and GaO_x, on ZSM-5-mediated polyolefin hydrocracking and identified GaO_x as a selective promoter for light gas formation. Incorporation of gallium oxide (3 wt % Ga) was shown to increase propane selectivity from 40 c-wt %, achieved over ZSM-5, to near 60 c-wt %, reaching a combined propane and butane selectivity of 85 c-wt %, while maintaining solids conversion. To elucidate the role of gallium oxide, we used *ex situ* and *operando* characterization techniques to probe acidity, local coordination environment, and the spatial distribution of GaO_x species. Extra-framework gallium oxide introduced via incipient wetness impregnation reduced the measured acid site density from 1275 to 911 μmol g^{-1}, decreased the Brønsted/Lewis acid site ratio, and formed a high-coverage GaO_x layer on the external surface of the zeolite. *Operando* experiments show that Ga is present in both Ga^{3+} and Ga^{1+} under reaction conditions. Attempts to disperse gallium oxide through reductive pretreatments led to an increase in the Lewis acid site concentration and a 10 c-wt % decrease in propane selectivity, highlighting the importance of the specific location, structural, and acidic configurations. Systematic variation of impregnation methods to control location and dispersion revealed a synergistic interaction between gallium oxide and zeolite acid sites, with propane selectivity strongly influenced by spatial proximity of GaO_x to acid sites. Furthermore, vapor-phase flow reactions with a model compound demonstrated a decrease in intermediate product formation compared to the zeolite alone. The optimized catalyst was validated across diverse polyolefin substrates and resulted in similar increases to propane selectivity, yielding >80 c-wt % combined C_3−C_4 selectivity across the range of polyolefin substrates.



KEYWORDS: *plastics deconstruction, polyethylene, hydrocracking, ZSM-5, gallium oxide*

INTRODUCTION

The heterogeneous hydrocracking of polyolefins provides a catalytic route for converting plastic waste into value-added hydrocarbons under relatively mild conditions.[1−4] Hydrocracking employs Brønsted acids, either alone or together with metallic sites in bifunctional catalysts, to generate carbocation intermediates that undergo isomerization and β-scission, resulting in a product distribution that depends on the balance between metallic and acidic functionalities.[5−7] Our previous process modeling study of polyethylene (PE) hydrocracking identified optimal target products and key process drivers,[8] suggesting that C_3−C_4 alkenes were favorable products in terms of both economics and reduced greenhouse gas (GHG) emissions relative to primary production. Experimentally, a 70% combined yield of propane, isobutane, and butane is achievable using ZSM-5 zeolite[5,9] (Figure 1), and this product mixture was modeled as the feedstock for dehydrogenative upgrading with the CATOFIN process. The resulting propylene minimum selling price (MSP) was competitive with virgin propylene, and although most life cycle impacts improved relative to primary production, GHG emissions remained comparable. Sensitivity analysis identified product yield as a key process variable, with a 20% increase in yield resulting in 30% and 44% reductions in MSP and GHG emissions, respectively, motivating the development of catalysts that can further enhance propane and butane formation.

Most efforts to tune polyolefin hydrocracking selectivity have focused on bifunctional metal-acid catalysts containing Ru, Pt, Ni, or Co.[1−7,10,11] These metals promote hydrogenolysis and hydrogenation but also favor methanation and liquid-range products, particularly at high metal loadings, large particle sizes, or elevated temperatures. Consequently, extensive efforts have

Received: August 19, 2026
Revised: September 21, 2026
Accepted: October 6, 2026

Downloaded from pubs.acs.org/acscatal/article-pdf/doi/10.1021/acscatal.6c06722/6897313/cs-2026-067228.pdf?guestAccessKey=2e356292-6312-461c-9958-d129ff7cd027 by MASSACHUSETTS INST OF TECHNOLOGY user on 26 October 2026

© XXXX American Chemical Society

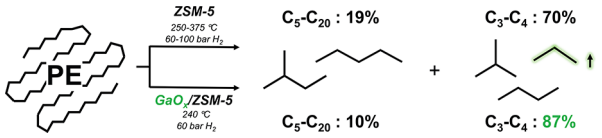


Figure 1. Overview on ZSM-5 hydrocracking to selective light alkane products.

focused on tuning the particle size, dispersion, electronic structure, promoters, and supports to favor liquid-range products.[6,7,12−27] Brønsted acidic zeolites are frequently used as supports, but above temperatures of 200 °C, zeolites alone are catalytically active for polyolefin hydrocracking,[5,11,28−30] with medium-pore zeolites preferentially producing light gases, whereas large- or extra-large-pore zeolites favor gasoline-range hydrocarbons.[26,31−36] Attempts to combine metals with medium-pore zeolites to enhance hydrogen activation while preserving acid-mediated selectivity have been reported to shift products to higher carbon numbers or decrease hydrocracking activity relative to the parent zeolite,[5,11] suggesting that alternative dopants that increase C−H activation without overwhelming zeolite-mediated cracking pathways may be worthy of further study.

To that end, promoters used in light alkane dehydrogenation provide a potential approach to decouple hydrogen activation from extensive C−C cleavage. Pt and Cr oxides exhibit high activity for light alkane dehydrogenation where promoters such as Sn, Zn, Ga, and In are used to suppress side reactions and stabilize active sites.[37,38] Gallium in particular, which is used to promote dehydrogenation, aromatization, or cracking, can be introduced into ZSM-5 via hydrothermal synthesis, ion exchange, vapor-phase exchange, or impregnation, with each method generating distinct gallium species that exhibit different catalytic functions.[39−43] Moreover, Ga and Zn have been extensively studied as dopants on ZSM-5 for both cracking and hydrocarbon aromatization.[44,45] Recently, Qian et al. reported aromatization of HDPE and PP over Ga-promoted zeolites, achieving a yield of 60% BTEX (benzene, toluene, ethylbenzene, and xylenes).[46] Incorporation of Ga introduces Lewis acidic sites that facilitate hydrogen transfer and dehydrogenation, while Brønsted acid sites promote cracking.[44] Numerous other studies have investigated the influence of Ga and Zn on olefin selectivity from various alkanes,[47−50] along with additional work evaluating polyolefin cracking to gasoline-range products.[51−53] However, these dopants have not been systematically evaluated in combination with zeolites to enhance light hydrocarbon hydrocracking selectivity.

In this study, motivated by the well-established influence of dopants on the dehydrogenation of light alkanes and their limited application in polyolefin hydrocracking, we examined the role of metal/metal oxides in enhancing polyolefin hydrocracking selectivity toward light hydrocarbons. We demonstrate that extra-framework gallium oxide selectively enhances propane formation during polyolefin hydrocracking using ZSM-5. Using low Si/Al ZSM-5 (Si/Al = 11.5) as a baseline catalyst, we show that incorporation of gallium oxide (3 wt % Ga) increases C_3−C_4 selectivity by 15 c-wt % without decreasing solids conversion (Figure 1). Propane selectivity depends strongly on gallium oxide location, with extra-framework GaO_x introduced by incipient wetness impregnation yielding the highest propane selectivity, approaching 60 c-wt %. Comprehensive *ex situ* and *operando* characterization studies were conducted to elucidate the changes in acidity, gallium oxidation state, gallium coordination environment, and spatial distribution that correlate with this selectivity enhancement.

RESULTS

Influence of Metal Oxide Species on Polyolefin Hydrocracking

PE hydrocracking was first evaluated over a commercial ZSM-5 catalyst with Si/Al = 11.5 (Table S1), to establish a base case and enable a direct comparison with our prior process modeling study.[8] Reactions conducted at 240 °C, 40 bar H_2, and 16 h resulted in 66% solids conversion and a recovered carbon propane selectivity of 32 c-wt %. To assess how dopants modify activity and selectivity, a series of metals and metal oxides were added onto ZSM-5 via incipient wetness impregnation (IWI). All catalysts were evaluated at a fixed total dopant loading of 3 wt % and constant reaction time to isolate the influence of dopant identity on solids conversion and product distribution (Figure 2).

Pt was selected as a benchmark dopant due to its widespread use in bifunctional hydrocracking catalysts and its well-established hydrogenation and hydrogenolysis activity.[1,11,25] Incorporation of 3 wt % Pt on ZSM-5 decreased solids conversion relative to the parent zeolite and decreased propane selectivity from 32 to 23 c-wt %, while selectivity toward iC_5, nC_5, and C_{6+} products increased (Figure 2). Similar reductions in activity upon metal addition have been reported previously, even at lower metal loadings.[5,11] The Pt-containing catalyst primarily produced *n*-alkane and *iso*-alkane products, consistent with Pt-mediated C−C bond cleavage occurring in parallel with hydrogenation and dehydrogenation. Based on prior reports that Sn modified both the ensemble size and the electronic structure of Pt, Sn was subsequently added as a promoter at 0.5 wt % with Pt.[38] Although Pt−Sn systems have improved activity in other hydrocracking studies,[25] incorporation of Sn

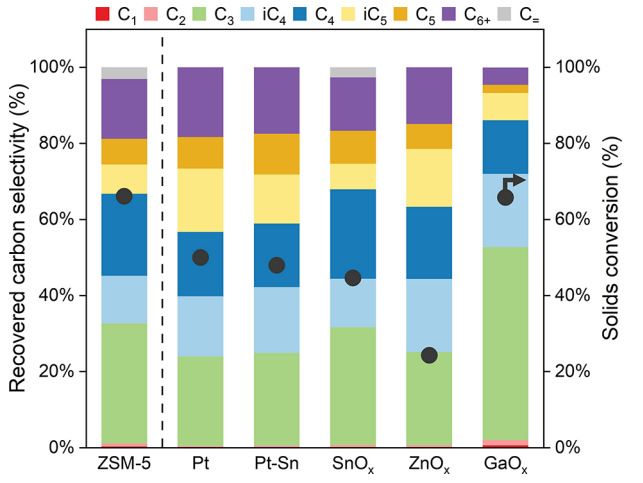


Figure 2. Recovered carbon selectivity and solids conversion for the reaction of metal/metal oxide on ZSM-5 Si/Al = 11.5 (Pt, Pt-Sn, SnO_x, GaO_x, and ZnO_x). Reaction conditions: 700 mg of PE 4k, 46 mg of catalyst total, 3 wt % metal/metal oxide loading, 240 °C, 16 h, 40 barg of H_2 fill at room temperature, 600 rpm, 1 h heat ramp. The Pt-Sn catalyst had a weight loading of 3 wt % Pt and 0.5 wt % Sn. ZSM-5 and GaO_x/ZSM-5 are averages of triplicate experiments (Figure S1). All data shown graphically here are provided in Excel S1.

https://doi.org/10.1021/acscatal.6c06722
ACS Catal. XXXX, XXX, XXX−XXX

Downloaded from pubs.acs.org/acscatal/article-pdf/doi/10.1021/acscatal.6c06722/6897313131/cs-2026-067228.pdf?guestAccessKey=2e356292-6312-461c-9958-d129ff7cd027 by MASSACHUSETTS INST OF TECHNOLOGY user on 26 October 2026

with Pt on ZSM-5 did not alter conversion or selectivity relative to Pt alone under the conditions studied here (Figure 2).

Metal oxides without noble metals exhibited mixed effects on hydrocracking performance. Tin oxide and zinc oxide did not increase solids conversion or propane selectivity relative to ZSM-5, and zinc oxide reduced solids conversion by 42%. In contrast, the addition of gallium oxide (3 wt % Ga) yielded 66% solids conversion, while increasing propane selectivity by approximately 19 c-wt % relative to the carrier. This increase occurred primarily at the expense of heavier products, with C_{6+} recovered carbon selectivity decreasing from 16 c-wt % for the ZSM-5 carrier to 5 c-wt % for GaO_x-modified ZSM-5, indicating that GaO_x selectively promotes pathways that favor light alkane formation without suppressing zeolite-mediated cracking activity.

The total acid site counts measured by NH_3-TPD are provided in Table S2 with individual profiles provided in Figure S4. All catalysts exhibited two desorption features corresponding to weak and strong acid sites. Although NH_3-TPD cannot distinguish between Brønsted and Lewis acid sites, the total acid site densities were similar across samples, averaging ~1000 μmol NH_3 adsorbed g^{-1}. The reducibility of the gallium oxide catalyst was probed via H_2-TPR (Figure S5), wherein a weak reduction feature was observed near 500 °C, with no additional reduction up to 1000 °C. Prior studies have attributed such low temperature reduction behavior to highly dispersed gallium species, whereas bulk Ga_2O_3 typically reduces near 900 °C.[41,54−56] Based on its unique propane selectivity enhancement and preserved activity, gallium oxide was selected for further optimization and characterization.

Evaluation of the GaO_x/ZSM-5 Bifunctional System

To evaluate the influence of acidity on activity and selectivity in the bifunctional system, a different parent zeolite, with a higher Si/Al ratio of 40 (Table S1, Zeolyst, Si/Al = 40), was evaluated due to its lower total acidity. NH_3-TPD analysis shows that the Si/Al = 40 contains approximately three times fewer acid sites than Si/Al = 11.5 (348 μmol g^{-1} vs 1275 μmol g^{-1}, respectively; Table S3 and Figure S6). Despite this difference, ZSM-5 Si/Al = 40 achieved nearly the same solids conversion as Si/Al = 11.5 under base-case conditions (60% vs 66%; Figure 3A) but exhibited drastically different product selectivity (Figure 3B). Introducing GaO_x to ZSM-5 Si/Al = 40 (3 wt % Ga) increased propane selectivity by ~8 c-wt %, but this increase occurred alongside a decrease in solids conversion (Figure 3A,B). Extending the reaction time to 48 h improved solids conversion to ~80%, while propane selectivity increased by only ~7 c-wt % (Figure S7). A slightly smaller crystallite size was observed for ZSM-5 Si/Al = 40 compared to Si/Al = 11.5 (Figure S8), which may contribute to the observed changes in product selectivity. Additionally, a higher concentration of acid sites could enable intermediates to encounter multiple active sites, promoting secondary cracking to terminal products.

To assess the bifunctional system without zeolite confinement, an amorphous silica-alumina support (SIRAL40HPV, Table S1) was examined due to its similar total acid site density to ZSM-5 Si/Al = 40 (371 μmol g^{-1} vs 348 μmol g^{-1}, respectively; Table S3 and Figure S6). Both the parent and GaO_x-modified SIRAL catalysts exhibited minimal solids conversion and negligible product formation under base-case conditions (Figure 3). Increasing the reaction time to 48 h did not significantly increase activity (Figure S9). NH_3-TPD showed a single desorption feature centered near 250 °C, indicating predominantly weak acid sites and a distinctly lower acid strength than that of the zeolite. Thus, similar total acid site densities alone are insufficient to replicate the catalytic behavior of ZSM-5. Given that the SIRAL and zeolite supports differ in pore structure, crystallinity, and confinement, the individual contributions of these properties cannot be deconvoluted when comparing both materials. Based on its activity and enhancement in propane selectivity, GaO_x/ZSM-5 (Si/Al = 11.5) was selected for detailed catalytic analysis and structural characterization.

To distinguish the contributions of framework and extra-framework gallium species in the GaO_x/ZSM-5 (Si/Al = 11.5) catalyst, a series of materials containing gallium in distinct structural environments were prepared and evaluated. The commercial ZSM-5 (Si/Al = 11.5) (Al-ZSM-5), which contains framework Al but no gallium, achieved 66% solids conversion and primarily produced C_3−C_5 hydrocarbons under base-case conditions (Figure 4). To assess the role of framework Ga species in PE hydrocracking, a gallosilicate (Ga-ZSM-5) was hydrothermally synthesized with a Si/Ga ratio of 41 using an adapted literature procedure reported to yield predominantly framework-incorporated Ga species.[42] This material exhibited reduced activity (27% solids conversion) and enhanced selectivity toward C_{7+} products (Figure 4).

Comparing the Ga-ZSM-5 to a commercial Al-ZSM-5 with similar acid site density, Si/Al = 40, catalytic evaluation confirmed that Al-ZSM-5 still achieved higher solids conversion and greater selectivity toward C_3−C_4 hydrocarbon species than Ga-ZSM-5 (Figure S10C). SEM indicated a smaller aggregate particle size for the gallosilicate material relative to the commercial aluminosilicate (Figure S11). The NH_3-TPD profiles exhibited similar acid site densities for both Ga-ZSM-5 and Al-ZSM-5 Si/Al = 40 (348 μmol g^{-1} for Al-ZSM-5 vs 293 μmol g^{-1} for Ga-ZSM-5; Table S4 and Figure S10A), with the gallosilicate also exhibiting a lower desorption temperature, consistent with weaker acid sites. To further probe the effect of framework species, a material containing both Al and Ga in-framework was hydrothermally synthesized with a Si/Al ratio of 19 and a Si/Ga ratio of 145. This sample had a measured acid site density of 775 μmol g^{-1}, consistent with the increase in the Si/Al ratio, and achieved near-complete solids conversion (96%) (Figure S10C and Table S4). TEM confirmed that Ga was well-dispersed throughout the sample (Figure S11D). However, its product selectivity was still less than that of the commercial aluminosilicate with Si/Al = 11.5, reinforcing that the Ga species most effective for enhancing light-gas selectivity in PE hydrocracking are those introduced as extra-framework.

To isolate the role of extra-framework gallium oxide, we evaluated a series of supported catalysts prepared using different deposition strategies. First, gallium oxide supported on silica (GaO_x/SiO_2) was prepared via IWI to decouple gallium oxide chemistry from zeolite acidity. TEM (Figure S12) showed the absence of GaO_x agglomerations. Catalytic evaluation of GaO_x/SiO_2 resulted in negligible product formation (Figure 4). A physical mixture (Mix) of GaO_x/SiO_2 and ZSM-5 (Si/Al = 11.5) achieved solids conversion identical to ZSM-5 (Si/Al = 11.5) (Al-ZSM-5) alone and exhibited a similar product distribution, demonstrating that close spatial proximity between gallium oxide and zeolite acid sites is required to promote selectivity enhancements (Figure 4).

Gallium oxide was next deposited directly onto ZSM-5 (Si/Al = 11.5) using different preparation methods. Gallium oxide introduced via IWI resulted in solids conversion comparable

Downloaded from pubs.acs.org/acscatal/article-pdf/doi/10.1021/acscatal.6c06722/6897313131/cs-2026-067228.pdf?guestAccessKey=2e356292-6312-461c-9958-d129ff7cd027 by MASSACHUSETTS INST OF TECHNOLOGY user on 26 October 2026

https://doi.org/10.1021/acscatal.6c06722
ACS Catal. XXXX, XXX, XXX−XXX

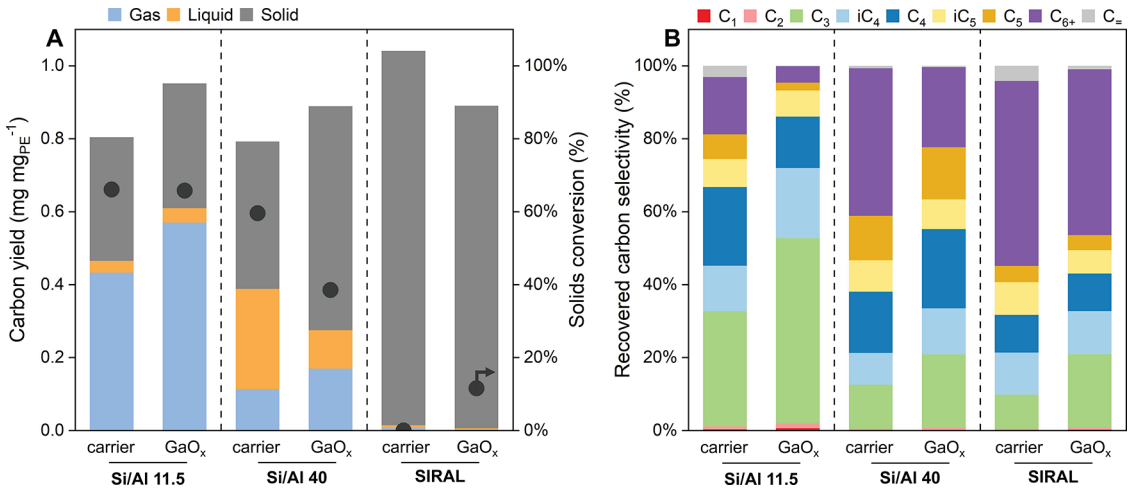


Figure 3. (A) Phase yield and solids conversion and (B) recovered carbon selectivity for reaction over carriers ZSM-5 Si/Al = 11.5, ZSM-5 Si/Al = 40, and SIRAL Si/Al = 0.3 with and without GaO_x. GaO_x was added to the carrier via IWI (3 wt % Ga). Reaction conditions: 700 mg of PE 4k, Si/Al = 11.5 = 46 mg of catalyst, Si/Al = 40 = 48 mg of catalyst, SIRAL Si/Al = 0.3 = 47 mg of catalyst, 240 °C, 16 h, 40 barg of H_2 fill at room temperature, 600 rpm, 1 h ramp. ZSM-5 Si/Al = 11.5 and GaO_x/ZSM-5 Si/Al = 11.5 are averages of triplicate experiments (Figure S1). All data shown graphically here are provided in Excel S1.

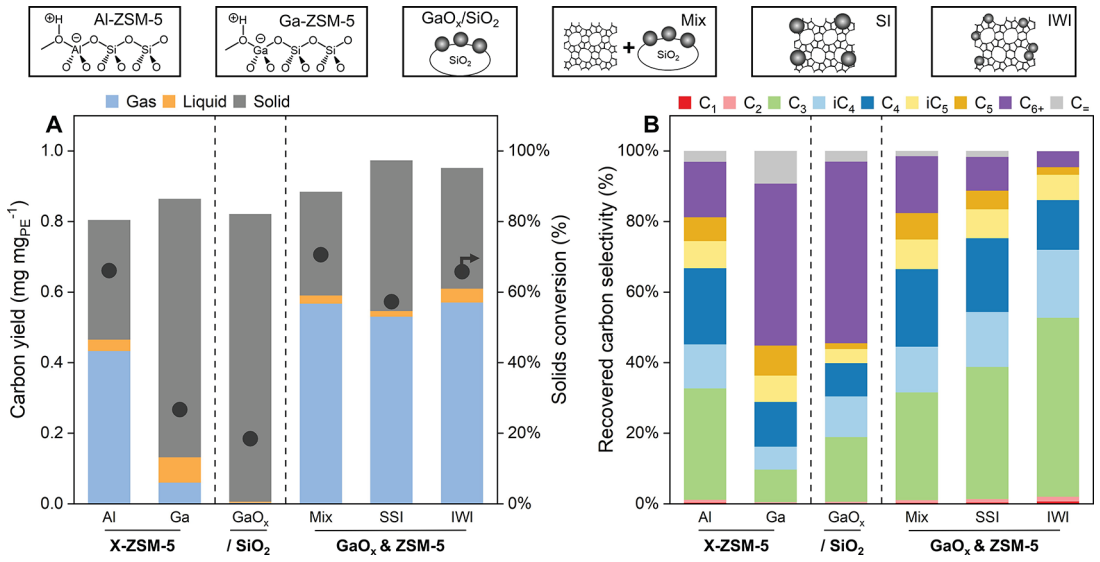


Figure 4. (A) Phase yield and solids conversion and (B) recovered carbon selectivity for reaction over the catalyst with different Ga speciation. Al-ZSM-5: 46 mg of ZSM-5 Si/Al = 11.5. Ga-ZSM-5: 50 mg of hydrothermally synthesized gallosilicate, Si/Ga = 41. GaO_x/SiO_2: 49 mg of GaO_x/SiO_2 (3 wt % Ga IWI). Mix: 49 mg of GaO_x/SiO_2 3 wt % Ga IWI + 43 mg of ZSM-5 Si/Al = 11.5. SSI: 46 mg of GaO_x/ZSM-5 Si/Al = 11.5 (3 wt % Ga SSI). IWI: 46 mg of GaO_x/ZSM-5 Si/Al = 11.5 (3 wt % Ga IWI). Reaction conditions: 700 mg of PE 4k, 240 °C, 16 h, 40 barg of H_2 fill at room temperature, 600 rpm, 1 h ramp. Al-ZSM-5 (ZSM-5 Si/Al = 11.5) and IWI (GaO_x/ZSM-5 Si/Al = 11.5) are averages of triplicate experiments (Figure S1). All data shown graphically here are provided in Excel S1.

to the carrier alone but significantly suppressed C_{6+} products while enhancing propane selectivity, as demonstrated in Figure 2. Gallium oxide was then incorporated via solid-state ion exchange (SSI), a method similar to IWI but that does not require dissolving the precursor in water. As expected, SSI produced slightly larger, less dispersed gallium oxide species (Figure S13). The SSI sample performed between the physical mixture and IWI catalyst, consistent with the presence of larger, more agglomerated gallium oxide particles (Figure 4).

The influence of gallium oxide loading was next evaluated for catalysts prepared by IWI and SSI. For the IWI series, increasing the loading from 1 to 11 wt % increased solids conversion, reaching a maximum of 65% at 11 wt % (Figure S14). Product selectivity remained largely constant throughout the series, with maximum propane selectivity of approximately 50 c-wt % observed at 3 wt % Ga. For the SSI series, increasing loading from 3 to 23 wt % increased solids conversion to a maximum of 75% at 11 wt %, followed by a decline at higher loadings (Figure S15). Propane selectivity in this series remained lower, at ~40 c-wt %. TEM of selected samples showed increasing agglomeration of GaO_x species on the zeolite surface as loading increased for both IWI and SSI

https://doi.org/10.1021/acscatal.6c06722
ACS Catal. XXXX, XXX, XXX−XXX

Downloaded from pubs.acs.org/acscatal/article-pdf/doi/10.1021/acscatal.6c06722/6897313/cs-2026-067228.pdf?guestAccessKey=2e356292-6312-461c-9958-d129ff7cd027 by MASSACHUSETTS INST OF TECHNOLOGY user on 26 October 2026

(Figures S16 and S17). Acid site characterization by NH_3-TPD confirmed a reduction in total acid site density upon GaO_x incorporation (Tables S5 and S6), accompanied by a shift in the high-temperature desorption peak (Figures S18 and S19) for both impregnation methods. To distinguish between Brønsted and Lewis acid sites, pyridine adsorption infrared spectroscopy was performed on selected IWI samples. The ν(CCN) ring-stretching vibrations of chemisorbed pyridine (19b mode) were monitored, with bands at ~1545 cm^{-1} assigned to pyridinium ions on Brønsted acid sites (Pyr-H^+) and bands at ~1455 cm^{-1} assigned to pyridine coordinated to Lewis acid sites (Pyr-L).[57,58] The Brønsted/Lewis acid site ratio was shown to decrease from 5.4 for the parent zeolite to 3.3 and 2.3 for the 1 and 3 wt % Ga samples, respectively, and then remained essentially unchanged at 2.2 for the 6 wt % Ga sample (Table S7). The acid site density and Brønsted/Lewis ratio remained constant between the 3 and 6 wt % samples, indicating that further increases in gallium content have little effect on the acid site distribution and provide no catalytic improvement.

Taken together, these results suggest that extra-framework gallium oxide participates in chain activation but is not active alone for PE cracking. Instead, the results thus far suggest a synergy between gallium oxide and zeolite acid sites, with performance strongly influenced by spatial proximity or speciation of these sites. For enhancing light gas production, IWI appears optimal, increasing propane selectivity to 50 c-wt % and achieving a combined C_3−C_4 selectivity of approximately 85 c-wt %.

Characterization of GaO_x/ZSM-5 Prepared via IWI

Because gallium oxide incorporation distinctly influences PE hydrocracking product selectivity, understanding the structural characteristics of GaO_x and resulting catalytic implications is essential. Comprehensive characterization of the GaO_x/ZSM-5 Si/Al = 11.5 (3 wt % Ga IWI) was conducted to elucidate the acidity, coordination environment, and spatial distribution of gallium oxide. A decrease in total acid site strength and density was observed with the addition of GaO_x (1275 μmol g^{-1} vs 911 μmol g^{-1}, respectively; Figure 5A). This observation aligns with the literature, demonstrating the consumption of Brønsted acid sites and formation of Lewis acid sites associated with the extra-framework Ga^{3+} species.[59] Consistent with the NH_3-TPD results, GaO_x incorporation led to a progressive decrease in total acidity, with a larger reduction in the Brønsted acid concentration. As a result, the concentration of Brønsted acid sites dropped from 953 to 608 μmol g^{-1} (Table S7), indicating a substantial shift in the acid site distribution upon gallium addition.

The Ga K-edge XANES spectrum of as-prepared GaO_x/ZSM-5 was compared to that of β-Ga_2O_3 as a Ga^{3+} standard (Figure 5B). The similar absorption edge energies of both indicated that the oxidic gallium species in GaO_x/ZSM-5 were present as Ga^{3+}. To gain insight into the local structure of the GaO_x species as a function of the weight loading, *ex situ* XAS data were collected at the Ga K-edge. Comparing the XANES spectra, there was a clear change in the relative amount of octahedrally (GaO_6) and tetrahedrally (GaO_4) coordinated oxidic Ga species as a function of the weight loading, as indicated by the intensity change between the two maxima in the white line region (Figure S20).[40,60] The corresponding Ga K-edge EXAFS data were modeled (Figure S21 and Table S8), revealing an increasing average agglomerate size (as determined from the Ga−Ga coordination number) with increasing loading. Moreover, the data were modeled considering the relative amount of octahedral and tetrahedral Ga species. In β-Ga_2O_3, there is a 50:50 mix of octahedral and tetrahedral species, while GaO_4 dominated the as-prepared IWI series. The gradual decrease in the estimated GaO_4 fraction from 74% to 64% corresponded with increasing loading from 1 to 11 wt % (Table S8). The higher amount of tetrahedral Ga oxidic species in the catalysts is interpreted as the presence of dispersed and more isolated GaO_x moieties.

An *operando* XAS experiment was performed with GaO_x/ZSM-5 Si/Al = 11.5 (3 wt % Ga IWI) at 12 bar using *n*-dodecane as a model polyolefin in the vapor phase with the aim of probing the local structure of the Ga species under more relevant conditions. There was a small redshift in XANES spectra and a decrease in white line intensity as the catalyst was exposed to H_2 at 180 °C and then to the H_2 + dodecane mixture (Figure S22A). Additionally, there were corresponding changes in the EXAFS spectra, suggesting possible structural changes upon H_2 treatment (Figure S22B,C). When the reaction temperature was further increased from 180 to 250 °C and held for 2 h, the XAS spectrum was similar (Figure S23). XANES linear combination fitting (LCF) was used to estimate the amount of reduced Ga species. While the amounts are small, the LCF gave 2% of GaO_x sites to be Ga^{1+} in the 1.5 h H_2-exposed catalyst (Figure S24A) and about 6% Ga^{1+} at 2 h TOS (Figure S24B). As the temperature was ramped from 180 to 250 °C in the presence of H_2 and dodecane, the Ga^{1+} fraction increased from 3% to 5% (Table S9).

EXAFS modeling was performed to determine any structural changes between the as-prepared catalyst and the active hydrocracking catalyst at 250 °C. Under reaction conditions, the Ga−O scattering was best modeled with a single Ga−O scattering path at 1.87 ± 0.01 Å, suggesting that Ga^{3+} under reaction conditions is present exclusively in a tetrahedral coordination environment (Table S10 and Figure S25). The apparent Ga−O coordination number decreased under hydrocracking conditions, consistent with the presence of a fraction of highly disordered or EXAFS-silent reduced Ga species.[61] Operando XANES fitting indicated that this reduced Ga population remained a minority under the reaction conditions examined. No Ga hydride bands were detected by H_2-FTIR under reaction-relevant conditions (Figure S26). These measurements show that the catalyst contains predominantly tetrahedrally coordinated oxidic Ga together with a minority reduced Ga population, but do not establish which Ga species is responsible for the enhanced propane selectivity or rule out a contribution from the reduced Ga fraction.

Finally, high-resolution XPS was used to elucidate the local coordination environment of the surface gallium oxide species, with the Ga 2p spectra and fitting results shown in Figure 5C. The Ga 2p region reveals two distinct coordination environments, with peaks centered at binding energies of 1117 and 1120 eV. Other catalyst systems have shown similar behavior, where a binding energy value of ~1120 eV is typically attributed to dispersed Ga_2O_3 interacting with the zeolite framework, while the binding energy of 1117 eV is associated with more bulk-like Ga_2O_3.[41,55,62] As Ga oxide loading increases, the relative abundance of bulk-like Ga_2O_3 species also increases (Figure S27A). Consistently, XANES measurements revealed that higher GaO_x loadings correlate with a greater proportion of octahedrally coordinated gallium such that the shoulder at ~10,381 eV evolves into a sharp peak especially above 6 wt %

Downloaded from pubs.acs.org/acscatal/article-pdf/doi/10.1021/acscatal.6c06722/6897313131/cs-2026-067228.pdf?guestAccessKey=2e356292-6312-461c-9958-d129ff7cd027 by MASSACHUSETTS INST OF TECHNOLOGY user on 26 October 2026

https://doi.org/10.1021/acscatal.6c06722
ACS Catal. XXXX, XXX, XXX−XXX

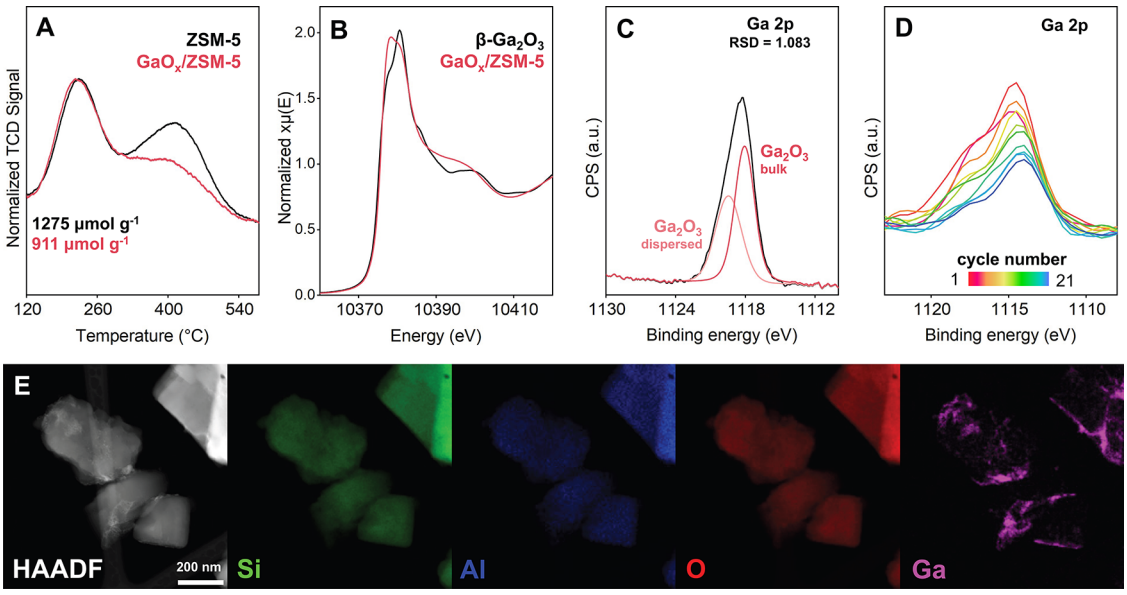


Figure 5. (A) NH_3-TPD profiles for ZSM-5 Si/Al = 11.5 (black) and GaO_x/ZSM-5 Si/Al = 11.5 (3 wt % Ga IWI) (pink). (B) XANES for β-Ga_2O_3 (black) and GaO_x/ZSM-5 Si/Al = 11.5 (3 wt % Ga IWI) (pink). (C) Ga 2p XPS spectra for GaO_x/ZSM-5 Si/Al = 11.5 (3 wt % Ga IWI). (D) Ga 2p XPS spectra after cycles of argon-ion gun sputtering (3000 V and 1 μA over a 2 × 2 mm^2 raster area). (E) HAADF-STEM image and corresponding EDS elemental mapping of Si (green), Al (blue), O (red), and Ga (purple) of GaO_x/ZSM-5 Si/Al = 11.5 (3 wt % Ga IWI).

Ga loading (Figure S20). EXAFS fits indicated higher octahedral gallium species and a trend toward higher Ga−Ga coordination with increased Ga loading, consistent with more bulk-like Ga_2O_3 species (Table S8).

Beyond the local coordination environment, the position and distribution of gallium oxide within the zeolite, as well as its proximity to acid sites, can strongly influence catalytic activity and selectivity. This was first probed using XPS depth profiling on a pristine sample, in which an argon-ion gun etched the surface (3000 V and 1 μA over a 2 × 2 mm^2 raster area) and spectra were collected after each sputtering cycle (Figure 5D). The intensity of Ga diminished with successive etching cycles, indicating a high concentration of surface gallium oxide species. This finding aligns with HAADF-STEM elemental mapping of the fresh catalyst (Figure 5E), which shows that Si, Al, and O are well-dispersed throughout the sample while Ga is enriched near the surface. Electron tomography further corroborates that Ga is predominantly located on the external surface of the zeolite (Figure S28).

Role of Extra-Framework Gallium Oxide in Supported Catalyst Systems

The influence of hydrogen on catalytic activity and product selectivity was evaluated by testing both the carrier and the GaO_x/ZSM-5 catalyst under identical conditions in the absence of H_2, using a fill pressure of 34 bar N_2. The resulting carbon yield, solids conversion, and recovered carbon selectivity are shown in Figure S29. At 240 °C, both catalysts were largely inactive (<10% product yield). Increasing the temperature to 250 and 260 °C improved carrier activity, whereas the GaO_x/ZSM-5 sample remained inactive (~10%). The lower activity under nitrogen is consistent with partial blocking of zeolite acid sites by GaO_x and/or the lack of activity by GaO_x in the absence of hydrogen. These results indicate that the promotional effect associated with GaO_x requires hydrogen; in its absence, the inhibitory effects associated with Ga incorporation on the underlying zeolite-mediated reaction pathway become dominant.

The influence of temperature and hydrogen pressure on catalytic performance was next evaluated for each catalyst system. ZSM-5 (Si/Al = 11.5) and the GaO_x/ZSM-5 (3 wt % Ga IWI) were tested at 230, 240, and 250 °C with solids conversion and recovered carbon selectivity shown in Figure S30. At 240 °C, both catalysts achieved high solids conversion (~75%) but exhibited markedly different propane selectivity, as previously noted. Increasing the reaction temperature to 250 °C resulted in complete solids conversion; however, propane selectivity for the carrier alone increased substantially (from 32 to 43 c-wt %) relative to the base-case condition, highlighting the importance of temperature in promoting cracking to terminal products. At 230 °C, the recovered carbon selectivity was nearly identical to that at 240 °C for both catalysts.

Subsequently, ZSM-5 (Si/Al = 11.5) and GaO_x/ZSM-5 IWI and SSI (3 wt %) samples were tested at 240 °C under varying hydrogen fill pressures (Figure S31). For ZSM-5, increasing hydrogen pressure moderately increased solids conversion while the recovered carbon selectivity remained relatively constant (Figure S31A). A similar trend was observed for the SSI and IWI samples, although a more substantial increase in activity occurred between 30 and 40 bar, with only marginal improvement at 50 bar (Figure S31B,C). Product selectivity for GaO_x-modified catalysts remained largely insensitive to hydrogen pressure across the range studied.

Product evolution during polyolefin hydrocracking was evaluated by varying reaction time from 2 to 48 h at 240 °C and 40 bar H_2 for both ZSM-5 (Figure 6A) and GaO_x/ZSM-5 (3 wt % Ga IWI) (Figure 6B). For ZSM-5, C_{6+} selectivity decreased with increasing reaction time, while propane formation increased. In contrast, the GaO_x/ZSM-5 exhibited a higher initial selectivity toward propane compared to the carrier.

https://doi.org/10.1021/acscatal.6c06722
ACS Catal. XXXX, XXX, XXX−XXX

Downloaded from pubs.acs.org/acscatcs/article-pdf/doi/10.1021/acscatal.6c06722/6897313131/cs-2026-067228.pdf?guestAccessKey=2e356292-6312-461c-9958-d129ff7cd027 by MASSACHUSETTS INST OF TECHNOLOGY user on 26 October 2026

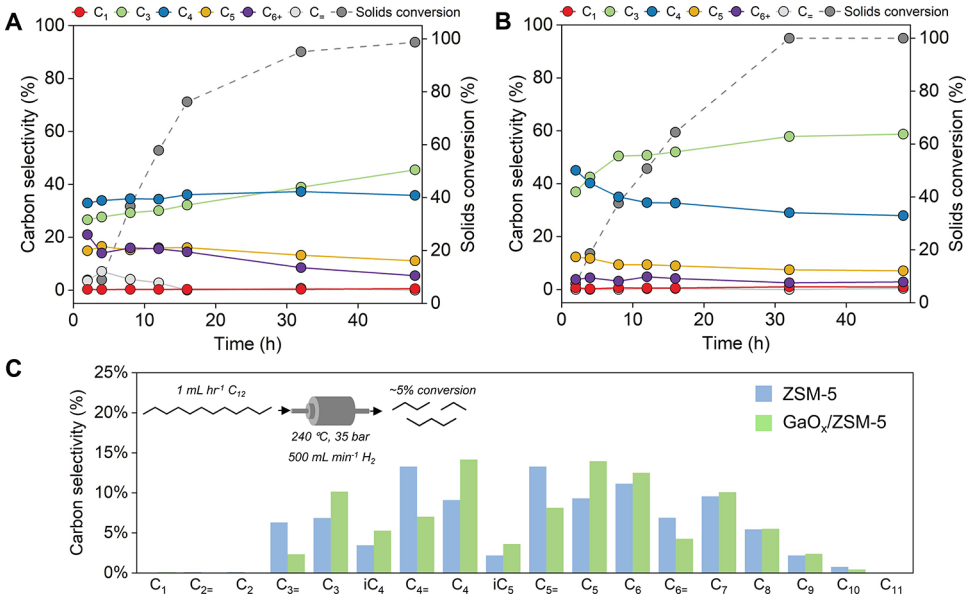


Figure 6. Effect of reaction time on the recovered carbon selectivity and solids conversion of (A) ZSM-5 Si/Al = 11.5 and (B) GaO_x/ZSM-5 Si/Al = 11.5 (3 wt % Ga IWI). Reaction conditions: 700 mg of PE 4k, 46 mg of catalyst total, 240 °C, 2−48 h, 40 barg of H_2 fill at room temperature, 600 rpm, 1 h heat ramp. (C) Recovered carbon selectivity for the continuous, vapor-flow model reaction of ZSM-5 Si/Al = 11.5 and GaO_x/ZSM-5 Si/Al = 11.5 (3 wt % Ga IWI). Reaction conditions: 1 mL h^{-1} *n*-dodecane, 23 mg of cat total, 275 mg of SiC, 240 °C, 35 barg, 500 mL min^{-1} H_2; bars are the averages of 5 GC injections collected at a steady state (~200 min). All data shown graphically here are provided in Excel S1.

Propane selectivity reached 50 c-wt % after 8 h and increased slightly, nearing 60 c-wt % after 32 h. At complete solids conversion, GaO_x/ZSM-5 achieved a combined propane and butane selectivity of 87 c-wt %. The selectivities to C_5 and C_{6+} products remained low for the GaO_x-modified catalyst throughout the experiment, indicating that its propane selectivity was less dependent on conversion over the range examined. For the parent ZSM-5, the increase in propane selectivity was more strongly associated with increasing conversion and the progressive cracking of heavier hydrocarbon intermediates.

Vapor-phase flow reactions with a model *n*-alkane (*n*-dodecane) were conducted to elucidate initial bond cleavage events and reaction pathways for both the carrier and the GaO_x-modified zeolite. Experiments were performed at a feed rate of 1 mL h^{-1} of *n*-dodecane and 500 mL min^{-1} of H_2 at 240 °C and 35 bar total pressure, achieving a steady state at approximately 5% dodecane conversion (Figure 6C). Consistent with batch results, ZSM-5 (Si/Al = 11.5) resulted in a product distribution that included more intermediate species, namely, alkene species. In contrast, the GaO_x-modified zeolite exhibited a higher selectivity toward light hydrocarbons (C_3, iC_4, and C_4) with reduced alkene selectivity. Both the selectivity of the carrier and the GaO_x-modified ZSM-5 varied with increasing contact time, consistent with more secondary cracking to increase selectivity of lighter species (Figure S32). These results further support the conclusion that gallium oxide incorporation promotes a distinct reaction pathway compared with the zeolite carrier. Both the time-resolved batch experiments and vapor-phase flow studies indicate that, at equivalent solids conversion and dodecane conversion, respectively, the parent zeolite generates a higher concentration of intermediate species, including higher-carbon-number hydrocarbons and olefins. In contrast, GaO_x alters the hydrocracking reaction network such that light alkanes are formed earlier, while higher-carbon-number and olefinic intermediates accumulate to a lesser extent, thereby shifting the product distribution toward C_3 and C_4 hydrocarbons.

Determining Active GaO_x Species for Enhanced Polyolefin Hydrocracking

Reductive pretreatments have been shown to modify the dispersion and coordination environment of Ga species in GaO_x-supported catalysts.[39,40,61,63] We therefore performed *in situ* XAS experiments under H_2-TPR conditions to monitor changes in Ga speciation during treatment. The XANES spectra showed the formation of Ga^{1+} at temperatures near 400 °C (Figure 7A).[64] At 400 °C, the estimated Ga^{1+} fraction reached 53% and increased to 70% after 1 h (Figure S33 and Table S12), whereas cooling to room temperature resulted in substantial reoxidation to Ga^{3+} (Figure S34).[61] These measurements show that the oxidation state of Ga is strongly dependent on the treatment temperature.

The catalyst reduced at 400 °C exhibited lower propane selectivity than the calcined catalyst (Figure 7B). This change cannot be assigned solely to the Ga oxidation state or Ga location because the pretreatment also modified Ga dispersion and the acid properties of the zeolite. NH_3-TPD showed a shift in the high-temperature desorption feature, consistent with a change in acid strength (Figure 7C). Pyridine-FTIR showed that the concentration of strong Brønsted acid sites remained nearly unchanged after reduction, whereas the concentration of strong Lewis acid sites increased from 199 to 346 μmol g^{-1} (Table S13). STEM-EDS further showed deeper penetration and greater dispersion of Ga species after reduction (Figure 7D,E), while N_2-physisorption indicated no substantial change in pore accessibility (Table S14). These results indicate that the reduction treatment produces a coupled change in Ga distribution and acid-site environment. The lower propane

https://doi.org/10.1021/acscatal.6c06722
ACS Catal. XXXX, XXX, XXX−XXX

Downloaded from pubs.acs.org/acscatcs/article-pdf/doi/10.1021/acscatal.6c06722/6897313131/cs-2026-067228.pdf?guestAccessKey=2e356292-6312-461c-9958-d129ff7cd027 by MASSACHUSETTS INST OF TECHNOLOGY user on 26 October 2026

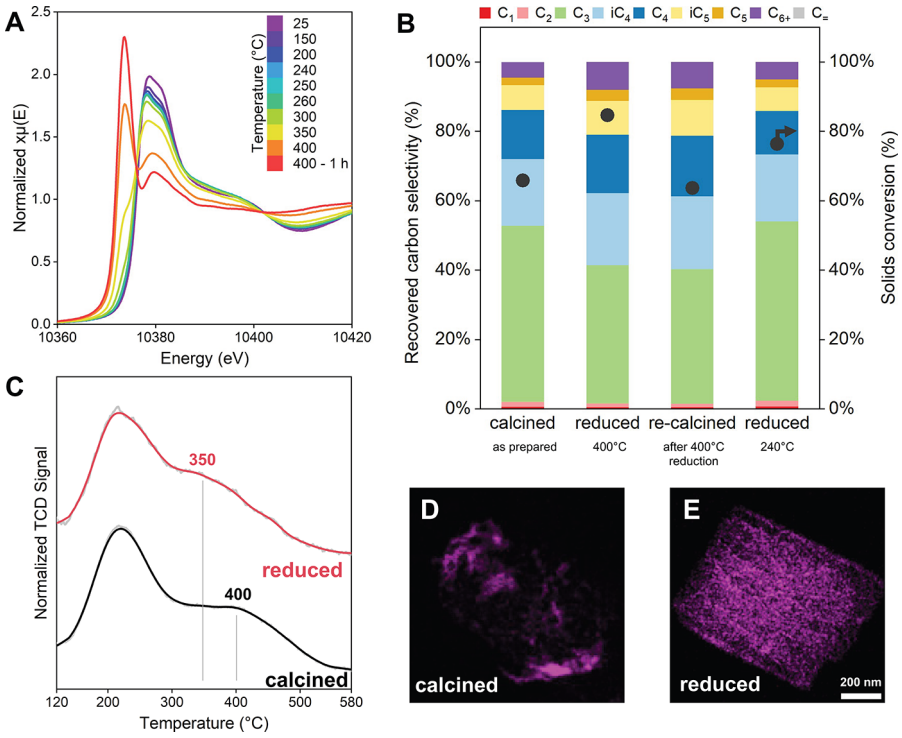


Figure 7. (A) Ga K-edge XANES spectra for GaO_x/ZSM-5 Si/Al = 11.5 (3 wt % Ga IWI) under temperature-programmed reduction. (B) Recovered carbon selectivity and solids conversion of GaO_x/ZSM-5 Si/Al = 11.5 (3 wt % Ga IWI) with different pretreatments (calcined, reduced at 400 °C, recalcined after reduction at 400 °C, and reduction at 240 °C). Reaction conditions: 700 mg of PE 4k, 46 mg of catalyst total, 240 °C, 16 h, 40 barg of H_2 fill at room temperature, 600 rpm, 1 h heat ramp. Calcined GaO_x/ZSM-5 Si/Al = 11.5 data are averages of triplicate experiments (Figure S1). All data shown graphically here are provided in Excel S1. (C) NH_3-TPD profiles of calcined GaO_x/ZSM-5 Si/Al = 11.5 (3 wt % Ga IWI) (black) and after reduction at 400 °C (pink). (D) STEM-EDS Ga elemental map (purple) of GaO_x/ZSM-5 Si/Al = 11.5 (3 wt % Ga IWI) as-synthesized (calcined). (E) STEM-EDS Ga elemental map (purple) of GaO_x/ZSM-5 Si/Al = 11.5 (3 wt % Ga IWI) after reduction at 400 °C (3 h, 100 mL min^{-1} H_2).

selectivity is therefore consistent with a change in the combined Ga-acid-site configuration, although the individual contribution of Ga location, coordination, oxidation state, and acidity cannot be separated by this experiment alone.

To confirm these observations, the catalyst was pretreated in H_2 again, this time at reaction temperature (100 mL min^{-1} H_2, 240 °C, 3 h) to better replicate the hydrocracking environment. XANES analysis showed no evidence of reduction at 240 °C (Figure 7A), and catalytic performance was unchanged when compared to the as-prepared, calcined sample (Figure 7B). At typical hydrocracking temperatures between 240 and 260 °C, Ga^{1+} appeared to be the minor species with an estimated 5−6% fraction. Note that the Ga^{1+} fraction estimate for the *operando* experiment at 250 °C in the presence of dodecane was also around 5%; therefore, the catalyst reduced(with H_2 only) at 240 °C is expected to have a similar structure to the active catalyst at 240 °C with the majority of GaO_x species as Ga^{3+}. This expectation correlates with similar catalytic performance of calcined and 240 °C reduced GaO_x/ZSM-5 as presented in Figure 7B. Furthermore, H_2-FTIR was conducted at 240 °C under flowing hydrogen (100 mL min^{-1}) to probe changes in GaO_x speciation under reaction-relevant conditions. Previous studies have demonstrated that Ga species exchange with Brønsted acid sites upon high-temperature (550−575 °C) reduction, as evidenced by the disappearance of Brønsted acid bands in FTIR and the loss of extra-framework Ga peaks in Ga MAS NMR.[39,40,63] Yuan et al. observed that in IWI samples with low Si/Al, the Ga^{11+} species resulting from the exchange can then interact with neighboring Brønsted acid sites to form hydride species.[63] After 4 h at reaction temperature, no hydride bands (2053 and 2037 cm^{-1}) were detected, and the Brønsted acid bands (3735, 3645, and 3591 cm^{-1}) remained unchanged (Figure S26) for the GaO_x/ZSM-5 catalyst.

Application to Other Polyolefin Substrates

As all catalytic trials utilized a model PE ($M_w \approx 4$ kDa), the optimized catalyst system was evaluated using other polyolefin substrates with varying sizes. Because the polyolefin substrates were purchased in a pellet form, they were cryomilled prior to reaction to ensure uniform particle size and improve catalyst contact. HT-GPC analysis before and after cryomilling confirmed no significant changes in molar mass or polydispersity occurred (Figure S35 and Table S15). The model PP 12k substrate exhibited a mass average molar mass (M_w) of 25 kDa, much higher than the reported value but consistent with literature observations.[65] The LDPE (25 MFI) and HDPE (2.2 MFI) provided higher-molar-mass substrates to evaluate, with measured values of 74 and 89 kDa, respectively.

The recovered carbon selectivity and solids conversion of PE, PP, LDPE, and HDPE using both ZSM-5 (Si/Al = 11.5) and GaO_x/ZSM-5 (3 wt % Ga IWI) under base-case conditions are shown in Figure 8. For PP and LDPE, the GaO_x-modified catalyst exhibited slightly lower solids conversion compared to

https://doi.org/10.1021/acscatal.6c06722
ACS Catal. XXXX, XXX, XXX−XXX

Downloaded from pubs.acs.org/acscacs/article-pdf/doi/10.1021/acscatal.6c06722/6897313131/cs-2026-067228.pdf?guestAccessKey=2e356292-6312-461c-9958-d129ff7cd027 by MASSACHUSETTS INST OF TECHNOLOGY user on 26 October 2026

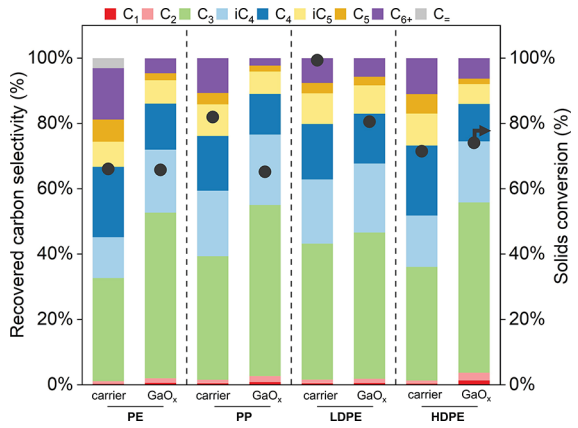


Figure 8. Recovered carbon selectivity and solids conversion for the reaction of PE, PP, LDPE, and HDPE using the carrier (ZSM-5 Si/Al = 11.5) and GaO_x/ZSM-5 Si/Al = 11.5 (3 wt % Ga IWI). Reaction conditions: 700 mg of PE 4k, 46 mg of catalyst total, 240 °C, 16 h, 40 barg of H_2 fill at room temperature, 600 rpm, 1 h heat ramp. The carrier (ZSM-5 Si/Al = 11.5) and GaO_x/ZSM-5 Si/Al = 11.5 (3 wt % Ga IWI) are averages of triplicate experiments (Figure S1). All data shown graphically here are provided in Excel S1.

the carrier. Despite the slight decrease in activity, the enhancement in propane remained consistent across the substrate series. For HDPE, a similar increase in propane selectivity (~15 c-wt %) was observed with GaO_x incorporation, comparable to the improvement seen for PE 4 kDa. After 16 h, both the HDPE and PE exhibited nearly identical product distributions, with a combined propane and butane selectivity of approximately 85 c-wt %. HT-GPC analysis of residual solids from HDPE and PE reactions exhibited a narrower molar mass distribution and a shift in the differential distribution toward higher molar masses, suggesting preferential cleavage of smaller chains (Figure S35). LDPE and PP showed smaller improvements in propane selectivity, which may be attributed to their highly branched structures, especially when compared to the linear structure of HDPE.

■ CONCLUSIONS

This work demonstrates that GaO_x-modified ZSM-5 selectively enhances light hydrocarbon formation during polyolefin hydrocracking. Guided by process modeling,[8] we evaluated several dopants for ZSM-5 and identified gallium oxide as promising, increasing propane selectivity by greater than 15 c-wt % when compared to the parent zeolite. PE time-series experiments and vapor-phase model compound studies suggest that GaO_x modification promotes a distinct pathway, where both sets of experiments showed a reduction in the formation of intermediate products relative to the parent zeolite. This enhanced selectivity requires the microporous environment of zeolite Brønsted acid sites, molecular hydrogen, and extra-framework gallium oxide species. Catalyst performance is strongly influenced by the GaO_x location, with incipient wetness impregnation yielding the highest propane selectivity. XPS depth profiling and STEM-EDS confirm GaO_x enrichment near the external surface, while acid site characterization indicates a decrease in the Brønsted/Lewis ratio upon GaO_x addition. These findings highlight GaO_x-modified ZSM-5 as a viable pathway for converting polyolefin waste into valuable light hydrocarbons, increasing propane selectivity to 60 c-wt % and resulting in a combined C_3−C_4 selectivity of 85 c-wt %.

■ MATERIALS AND METHODS

Materials

All substrates, commercial catalysts, and chemicals used in this study are provided in Table S1. The PE substrate (4000 Da M_w, Sigma-Aldrich) used throughout this text is a low-molecular weight model polyethylene-like wax that has been to shown to differ from commercial PE.[66−68]

Catalyst Preparation and Pretreatment

Commercial zeolite catalysts were calcined (550 °C, 5 h, 5 °C min^{-1} ramp rate, flowing air) and kept in sealed vials prior to use in reactions or further synthesis. Supported catalysts were prepared using IWI or SSI methods and then calcined (550 °C, 5 h, 5 °C min^{-1} ramp rate, flowing air) to yield metal oxide species. For Pt and Pt-Sn, samples were reduced in flowing H_2 (100 mL min^{-1}) at 400 °C for 3 h and then passivated in air prior to use. Gallosilicate and galloaluminosilicate materials were prepared via hydrothermal synthesis to include Ga or both Al and Ga in the framework, respectively. Further details on the catalyst preparation, including impregnation and hydrothermal synthesis, are provided in the Supporting Information.

Characterization

Substrates and postreaction solids were characterized via high-temperature gel permeation chromatography (HT-GPC).[69] Catalysts were characterized using ammonia temperature-programmed desorption (NH_3-TPD) and pyridine fourier-transform infrared spectroscopy (FTIR) for acid site quantification, hydrogen-temperature-programmed reduction (H_2-TPR) to probe reduction behavior, scanning transmission electron microscopy (STEM) and scanning electron microscopy (SEM) to assess catalyst morphology and particle distribution, powder X-ray diffraction (PXRD) to verify zeolite crystallinity, nitrogen physisorption (N_2-physisorption) was used to determine surface area and micropore volume, and inductively coupled plasma−mass spectrometry (ICP-MS) to confirm metal/metal oxide loading. Additional details on the characterization techniques are provided in the Supporting Information.

Ex situ and *in situ*/*operando* X-ray absorption spectroscopy (XAS) experiments at the Ga K-edge were carried out at the Stanford Synchrotron Radiation Lightsource. Details on experimental procedures, beamline configuration, and *operando* setup (Scheme S1) are provided in the Supporting Information.

Reactivity Studies

In a typical batch reaction, a Parr reactor (25 mL, 316 SS) was loaded with 700 mg of PE (4000 Da M_w, Sigma-Aldrich) and 50 mg of the catalyst. TGA was used to measure the water content of the catalyst and correct the reactor mass loading (details in the Supporting Information). Catalyst loadings provided in figure captions reflect the water content. The sealed reactor was purged by three pressure cycles between 5 and 15 bar hydrogen and then charged to a final pressure of 40 bar (~60 bar working pressure). The reactor was placed in a heating block and ramped to the target temperature over 1 h, and after reaching the target temperature, the reaction time began from that point. After reaching the desired reaction time, the reactor was quenched in an ice bath and allowed to cool to room temperature. Product capture, identification, and quantification followed previously reported procedures, with additional details provided in the Supporting Information.[9]

Vapor-phase flow reactions with *n*-dodecane were conducted in a high-pressure, continuous-flow fixed-bed reactor. Hydrogen was supplied at 500 mL min^{-1} using a digital mass flow controller (Brooks). Liquid *n*-dodecane was delivered at 1 mL h^{-1} via a high-pressure syringe pump (Chemyx) and entered a heated mixing zone (210 °C, Cole Palmer Digi-Sense PID controller) where it was rapidly vaporized into the hydrogen carrier stream. 25 mg of the catalyst (150−180 μm)

Downloaded from pubs.acs.org/acscatal/article-pdf/doi/10.1021/acscatal.6c06722/6897313/cs-2026-067228.pdf?guestAccessKey=2e356292-6312-461c-9958-d129ff7cd027 by MASSACHUSETTS INST OF TECHNOLOGY user on 26 October 2026

https://doi.org/10.1021/acscatal.6c06722
ACS Catal. XXXX, XXX, XXX−XXX

was diluted in 275 mg of SiC (120 grit) and packed into a stainless-steel reactor tube with a K-type thermocouple positioned at the bed outlet for accurate temperature monitoring. The reaction was carried out at 240 °C, with bed temperature controlled by a PID controller (Cole Palmer Digi-Sense) and heated transfer lines maintained above 212 °C using variable transformers (Vevor) to prevent condensation. The reactor effluent passed through a heated back-pressure regulator (Equilibar) to maintain an upstream pressure of 35 bar. The depressurized stream was analyzed online using gas chromatography-flame ionization detection (GC-FID) and a DB-1 column (Agilent). Product samples were collected every 38 min over the entire run.

Metrics used to evaluate and compare catalyst performance include carbon yield (Y_i), solids conversion (X_{PE}), and recovered product selectivity (S_i). All performance metrics are defined in eqs 1−3:

$$Y_i = \frac{m_{C,i}}{m_{C,PE,\ initial}} \tag{1}$$

$$X_{PE} = 1 - \frac{m_{solids}}{m_{PE,\ initial}} \tag{2}$$

$$S_i = \frac{m_{recovered\ Ci}}{\sum_{x=1}^{33} m_{recovered\ Cx}} \tag{3}$$

■ ASSOCIATED CONTENT

Supporting Information

The supporting information is available free of charge at https://pubs.acs.org/doi/10.1021/acscatal.6c06722.

Chemicals used, experimental procedures and setup, catalyst characterization, and experiments (DOCX)

Source of data shown in the figures (XLSX)

■ AUTHOR INFORMATION

Corresponding Author

Yuriy Román-Leshkov − *Department of Chemical Engineering, Massachusetts Institute of Technology, Cambridge, Massachusetts 02139, United States;* orcid.org/0000-0002-0025-4233; Email: yroman@mit.edu

Authors

Anna E. Brenner − *Department of Chemical Engineering, Massachusetts Institute of Technology, Cambridge, Massachusetts 02139, United States;* orcid.org/0000-0003-3669-2515

Faisal H. Alshafei − *Department of Chemical Engineering, Massachusetts Institute of Technology, Cambridge, Massachusetts 02139, United States;* orcid.org/0000-0003-1808-1374

Juliana Lu-Yang − *Department of Chemical Engineering, Massachusetts Institute of Technology, Cambridge, Massachusetts 02139, United States*

Ozge D. Bozkurt − *Stanford Synchrotron Radiation Lightsource, SLAC National Accelerator Laboratory, Menlo Park, California 94025, United States; BOTTLE Consortium, Golden, Colorado 80401, United States*

Marcos G. Farpón − *Department of Chemical Engineering, Massachusetts Institute of Technology, Cambridge, Massachusetts 02139, United States*

Colum O'Leary − *Stanford Synchrotron Radiation Lightsource, SLAC National Accelerator Laboratory, Menlo Park, California 94025, United States; BOTTLE Consortium, Golden, Colorado 80401, United States*

Arun Asundi − *Stanford Synchrotron Radiation Lightsource, SLAC National Accelerator Laboratory, Menlo Park, California 94025, United States; BOTTLE Consortium, Golden, Colorado 80401, United States*

Bowei Liu − *Department of Chemical Engineering, Massachusetts Institute of Technology, Cambridge, Massachusetts 02139, United States;* orcid.org/0009-0008-8568-7775

Rachita Rana − *Department of Chemical Engineering, Massachusetts Institute of Technology, Cambridge, Massachusetts 02139, United States*

Griffin Drake − *Department of Chemical Engineering, Massachusetts Institute of Technology, Cambridge, Massachusetts 02139, United States*

Simon R. Bare − *Stanford Synchrotron Radiation Lightsource, SLAC National Accelerator Laboratory, Menlo Park, California 94025, United States; BOTTLE Consortium, Golden, Colorado 80401, United States;* orcid.org/0000-0002-4932-0342

Gregg T. Beckham − *BOTTLE Consortium, Golden, Colorado 80401, United States; Renewable Resources and Enabling Sciences Center, National Laboratory of the Rockies, Golden, Colorado 80401, United States;* orcid.org/0000-0002-3480-212X

Complete contact information is available at: https://pubs.acs.org/doi/10.1021/acscatal.6c06722

Notes

The authors declare no competing financial interest.

■ ACKNOWLEDGMENTS

Funding was provided by the U.S. Department of Energy, Office of Critical Minerals and Energy Innovation, Advanced Materials and Manufacturing Technologies Office (AMMTO) and Alternative Fuels and Feedstocks Office (AFFO). This work was performed as part of the Bio-Optimized Technologies to keep the Thermoplastics out of Landfills and the Environment (BOTTLE) Consortium and was supported by AMMTO and AFFO under Contract No. DE-AC36-08GO28308 with the National Laboratory of the Rockies (NLR) and DE-AC03-76SF00515 with the SLAC National Accelerator Laboratory, operated by Stanford University. The BOTTLE Consortium includes members from MIT, funded under Contract DE-AC36-08GO28308 with NLR. The views expressed in the article do not necessarily represent the views of the DOE or the U.S. Government. Work at the Molecular Foundry was supported by the Office of Science, Office of Basic Energy Sciences, of the U.S. Department of Energy under Contract No. DE-AC02-05CH11231, under proposal number MFP-10179. Co-ACCESS, part of the SUNCAT Center for Interface Science and Catalysis, is supported by the U.S. Department of Energy, Office of Basic Energy Sciences, Chemical Sciences, Geosciences and Biosciences Division. Use of the Stanford Synchrotron Radiation Lightsource, SLAC National Accelerator Laboratory, is supported by the U.S. Department of Energy, Office of Science, Office of Basic Energy Sciences under Contract No. DE-AC02-76SF00515. Supplemental graphics were provided by BioRender. The authors thank Joel Miscall for assistance with HT-GPC,

Downloaded from pubs.acs.org/acscatal/article-pdf/doi/10.1021/acscatal.6c06722/6897313131/cs-2026-067228.pdf?guestAccessKey=2e356292-6312-461c-9958-d129ff7cd027 by MASSACHUSETTS INST OF TECHNOLOGY user on 26 October 2026

Emily Wu with ICP, and Anjani Maurya with XAS beamtime experiments. M.G.F. thanks Fundacion Ramon Areces for his postdoctoral fellowship.

REFERENCES

(1) Sun, J.; Dong, J.; Gao, L.; Zhao, Y. Q.; Moon, H.; Scott, S. L. Catalytic Upcycling of Polyolefins. *Chem. Rev.* **2024**, *124* (16), 9457−9579.

(2) Musa, A.; Jaseer, E. A.; Barman, S.; Garcia, N. Review on Catalytic Depolymerization of Polyolefin Waste by Hydrogenolysis: State-of-the-Art and Outlook. *Energy Fuels* **2024**, *38* (3), 1676−1691.

(3) Borkar, S. S.; Helmer, R.; Mahnaz, F.; Majzoub, W.; Mahmoud, W.; Al-Rawashdeh, M. m.; Shetty, M. Enabling resource circularity through thermo-catalytic and solvent-based conversion of waste plastics. *Chem. Catal.* **2022**, *2* (12), 3320−3356.

(4) Faust, K.; Denifl, P.; Hapke, M. Recent Advances in Catalytic Chemical Recycling of Polyolefins. *ChemCatChem* **2023**, *15* (13), No. e202300310.

(5) Lee, W. T.; van Muyden, A.; Bobbink, F. D.; Mensi, M. D.; Carullo, J. R.; Dyson, P. J. Mechanistic classification and benchmarking of polyolefin depolymerization over silica-alumina-based catalysts. *Nat. Commun.* **2022**, *13* (1), 4850.

(6) Vance, B. C.; Kots, P. A.; Wang, C.; Hinton, Z. R.; Quinn, C. M.; Epps, T. H.; Korley, L. T. J.; Vlachos, D. G. Single pot catalyst strategy to branched products via adhesive isomerization and hydrocracking of polyethylene over platinum tungstated zirconia. *Appl. Catal., B* **2021**, *299*, No. 120483.

(7) Rorrer, J. E.; Ebrahim, A. M.; Questell-Santiago, Y.; Zhu, J.; Troyano-Valls, C.; Asundi, A. S.; Brenner, A. E.; Bare, S. R.; Tassone, C. J.; Beckham, G. T.; Román-Leshkov, Y. Role of Bifunctional Ru/Acid Catalysts in the Selective Hydrocracking of Polyethylene and Polypropylene Waste to Liquid Hydrocarbons. *ACS Catal.* **2022**, *12* (22), 13969−13979.

(8) Yadav, G.; Uekert, T.; DesVeaux, J. S.; Van Roijen, E. C.; Rorrer, J. E.; Brenner, A. E.; Drake, G.; Zichittella, G.; Carlson, N.; Román-Leshkov, Y.; Beckham, G. T. Techno-economic analysis and life cycle assessment for the catalytic hydrogenolysis and hydrocracking of polyethylene. *Joule* **2026**, *10*, No. 102384.

(9) Brenner, A. E.; Drake, G.; Beckham, G. T.; Roman-Leshkov, Y. Methods for Carbon Mass Closure in Polyolefin Hydrocracking. *JACS Au* **2025**, *5* (8), 4123−4132.

(10) Rorrer, J. E.; Beckham, G. T.; Roman-Leshkov, Y. Conversion of Polyolefin Waste to Liquid Alkanes with Ru-Based Catalysts under Mild Conditions. *JACS Au* **2021**, *1* (1), 8−12.

(11) Tan, J. Z.; Hullfish, C. W.; Zheng, Y.; Koel, B. E.; Sarazen, M. L. Conversion of polyethylene waste to short chain hydrocarbons under mild temperature and hydrogen pressure with metal-free and metal-loaded MFI zeolites. *Appl. Catal., B* **2023**, *338*, No. 123028.

(12) Borkar, S. S.; Helmer, R.; Panicker, S.; Shetty, M. Investigation into the Reaction Pathways and Catalyst Deactivation for Polyethylene Hydrogenolysis over Silica-Supported Cobalt Catalysts. *ACS Sustainable Chem. Eng.* **2023**, *11* (27), 10142−10157.

(13) Chauhan, M.; Antil, N.; Rana, B.; Akhtar, N.; Thadhani, C.; Begum, W.; Manna, K. Isoreticular Metal-Organic Frameworks Confined Mononuclear Ru-Hydrides Enable Highly Efficient Shape-Selective Hydrogenolysis of Polyolefins. *JACS Au* **2023**, *3* (12), 3473−3484.

(14) Chen, L.; Moreira, J. B.; Meyer, L. C.; Szanyi, J. Efficient and selective dual-pathway polyolefin hydro-conversion over unexpectedly bifunctional M/TiO_2-anatase catalysts. *Appl. Catal., B* **2023**, *335*, No. 122897.

(15) Chen, S.; Tennakoon, A.; You, K.-E.; Paterson, A. L.; Yappert, R.; Alayoglu, S.; Fang, L.; Wu, X.; Zhao, T. Y.; Lapak, M. P.; Saravanan, M.; Hackler, R. A.; Wang, Y.-Y.; Qi, L.; Delferro, M.; Li, T.; Lee, B.; Peters, B.; Poeppelmeier, K. R.; Ammal, S. C.; Bowers, C. R.; Perras, F. A.; Heyden, A.; Sadow, A. D.; Huang, W. Ultrasmall amorphous zirconia nanoparticles catalyse polyolefin hydrogenolysis. *Nat. Catal.* **2023**, *6* (2), 161−173.

(16) Chu, M.; Wang, X.; Wang, X.; Lou, X.; Zhang, C.; Cao, M.; Wang, L.; Li, Y.; Liu, S.; Sham, T. K.; Zhang, Q.; Chen, J. Site-Selective Polyolefin Hydrogenolysis on Atomic Ru for Methanation Suppression and Liquid Fuel Production. *Research* **2023**, *6*, No. 0032.

(17) Chu, M.; Wang, X.; Wang, X.; Xu, P.; Zhang, L.; Li, S.; Feng, K.; Zhong, J.; Wang, L.; Li, Y.; He, L.; Cao, M.; Zhang, Q.; Chi, L.; Chen, J. Layered Double Hydroxide Derivatives for Polyolefin Upcycling. *J. Am. Chem. Soc.* **2024**, *146* (15), 10655−10665.

(18) Kang, Q.; Chu, M.; Xu, P.; Wang, X.; Wang, S.; Cao, M.; Ivasenko, O.; Sham, T. K.; Zhang, Q.; Sun, Q.; Chen, J. Entropy Confinement Promotes Hydrogenolysis Activity for Polyethylene Upcycling. *Angew. Chem., Int. Ed.* **2023**, *62* (47), No. e202313174.

(19) Kots, P. A.; Doika, P. A.; Vance, B. C.; Najmi, S.; Vlachos, D. G. Tuning High-Density Polyethylene Hydrocracking through Mordenite Zeolite Crystal Engineering. *ACS Sustainable Chem. Eng.* **2023**, *11* (24), 9000−9009.

(20) Lamb, J. V.; Lee, Y. H.; Sun, J.; Byron, C.; Uppuluri, R.; Kennedy, R. M.; Meng, C.; Behera, R. K.; Wang, Y. Y.; Qi, L.; Sadow, A. D.; Huang, W.; Ferrandon, M. S.; Scott, S. L.; Poeppelmeier, K. R.; Abu-Omar, M. M.; Delferro, M. Supported Platinum Nanoparticles Catalyzed Carbon-Carbon Bond Cleavage of Polyolefins: Role of the Oxide Support Acidity. *ACS Appl. Mater. Interfaces* **2024**, *16* (9), 11361−11376.

(21) Tamura, M.; Miyaoka, S.; Nakaji, Y.; Tanji, M.; Kumagai, S.; Nakagawa, Y.; Yoshioka, T.; Tomishige, K. Structure-activity relationship in hydrogenolysis of polyolefins over Ru/support catalysts. *Appl. Catal., B* **2022**, *318*, No. 121870.

(22) Tennakoon, A.; Wu, X.; Meirow, M.; Howell, D.; Willmon, J.; Yu, J.; Lamb, J. V.; Delferro, M.; Luijten, E.; Huang, W.; Sadow, A. D. Two Mesoporous Domains Are Better Than One for Catalytic Deconstruction of Polyolefins. *J. Am. Chem. Soc.* **2023**, *145* (32), 17936−17944.

(23) Vance, B. C.; Kots, P. A.; Wang, C.; Granite, J. E.; Vlachos, D. G. Ni/SiO_2 catalysts for polyolefin deconstruction via the divergent hydrogenolysis mechanism. *Appl. Catal., B* **2023**, *322*, No. 122138.

(24) Wang, C.; Xie, T.; Kots, P. A.; Vance, B. C.; Yu, K.; Kumar, P.; Fu, J.; Liu, S.; Tsilomelekis, G.; Stach, E. A.; Zheng, W.; Vlachos, D. G. Polyethylene Hydrogenolysis at Mild Conditions over Ruthenium on Tungstated Zirconia. *JACS Au* **2021**, *1* (9), 1422−1434.

(25) Wang, H.; Yoskamtorn, T.; Zheng, J.; Ho, P.-L.; Ng, B.; Tsang, S. C. E. Ce-Promoted PtSn-Based Catalyst for Hydrocracking of Polyolefin Plastic Waste into High Yield of Gasoline-Range Products. *ACS Catal.* **2023**, *13* (24), 15886−15898.

(26) Wu, X.; Wang, X.; Zhang, L.; Wang, X.; Song, S.; Zhang, H. Polyethylene Upgrading to Liquid Fuels Boosted by Atomic Ce Promoters. *Angew. Chem., Int. Ed.* **2024**, *63* (8), No. e202317594.

(27) Lu, S.; Jing, Y.; Jia, S.; Shakouri, M.; Hu, Y.; Liu, X.; Guo, Y.; Wang, Y. Enhanced Production of Liquid Alkanes from Waste Polyethylene via the Electronic Effect-Favored $C_{secondary}$−$C_{secondary}$ Bond Cleavage. *ChemCatChem* **2023**, *15* (3), No. e202201375.

(28) Bin Jumah, A.; Anbumuthu, V.; Tedstone, A. A.; Garforth, A. A. Catalyzing the Hydrocracking of Low Density Polyethylene. *Ind. Eng. Chem. Res.* **2019**, *58* (45), 20601−20609.

(29) Cen, Z.; Han, X.; Lin, L.; Yang, S.; Han, W.; Wen, W.; Yuan, W.; Dong, M.; Ma, Z.; Li, F.; Ke, Y.; Dong, J.; Zhang, J.; Liu, S.; Li, J.; Li, Q.; Wu, N.; Xiang, J.; Wu, H.; Cai, L.; Hou, Y.; Cheng, Y.; Daemen, L. L.; Ramirez-Cuesta, A. J.; Ferrer, P.; Grinter, D. C.; Held, G.; Liu, Y.; Han, B. Upcycling of polyethylene to gasoline through a self-supplied hydrogen strategy in a layered self-pillared zeolite. *Nat. Chem.* **2024**, *16* (6), 871−880.

(30) Duan, J.; Chen, W.; Wang, C.; Wang, L.; Liu, Z.; Yi, X.; Fang, W.; Wang, H.; Wei, H.; Xu, S.; Yang, Y.; Yang, Q.; Bao, Z.; Zhang, Z.; Ren, Q.; Zhou, H.; Qin, X.; Zheng, A.; Xiao, F. S. Coking-Resistant Polyethylene Upcycling Modulated by Zeolite Micropore Diffusion. *J. Am. Chem. Soc.* **2022**, *144* (31), 14269−14277.

Downloaded from pubs.acs.org/acscatsc/article-pdf/doi/10.1021/acscatal.6c06722/6897313131/cs-2026-067228.pdf?guestAccessKey=2e356292-6312-461c-9958-d129ff7cd027 by MASSACHUSETTS INST OF TECHNOLOGY user on 26 October 2026

https://doi.org/10.1021/acscatal.6c06722
ACS Catal. XXXX, XXX, XXX−XXX

(31) Han, X.; Zhou, X.; Ji, T.; Zeng, F.; Deng, W.; Tang, Z.; Chen, R. Boosting the catalytic performance of metal−zeolite catalysts in the hydrocracking of polyolefin wastes by optimizing the nanoscale proximity. *EES Catal.* **2024**, *2* (1), 300−310.
(32) Liu, S.; Kots, P. A.; Vance, B. C.; Danielson, A.; Vlachos, D. G. Plastic waste to fuels by hydrocracking at mild conditions. *Sci. Adv.* **2021**, *7* (17), No. eabf8283.
(33) Qiu, Z.; Lin, S.; Chen, Z.; Chen, A.; Zhou, Y.; Cao, X.; Wang, Y.; Lin, B. L. A reusable, impurity-tolerant and noble metal-free catalyst for hydrocracking of waste polyolefins. *Sci. Adv.* **2023**, *9* (25), No. eadg5332.
(34) Zhao, P.; Guo, W.; Gui, Z.; Jiang, J.; Zhu, Z.; Li, J.-J.; Zhao, L.; Zhou, J.; Xi, Z. Selective Hydrocracking of Waste Polyolefins toward Gasoline-Range Liquid Fuels via Tandem Catalysis over a Cerium-Promoted Pt/HY Catalyst. *ACS Sustainable Chem. Eng.* **2024**, *12* (15), 5738−5752.
(35) Zhou, X.; Han, X.; Qu, Z.; Zhang, J.; Zeng, F.; Tang, Z.; Chen, R. Hierarchical FAU Zeolites Boosting the Hydrocracking of Polyolefin Waste into Liquid Fuels. *ACS Sustainable Chem. Eng.* **2024**, *12* (15), 6013−6022.
(36) Han, X.; Zhang, J.; Qu, Z.; Ji, T.; Zeng, F.; Jiang, H.; Huang, J.; Tang, Z.; Xing, W.; Chen, R. Engineering noble metal-free nickel catalysts for highly efficient liquid fuel production from waste polyolefins under mild conditions. *Fuel* **2025**, *382*, No. 133733.
(37) Chen, S.; Chang, X.; Sun, G.; Zhang, T.; Xu, Y.; Wang, Y.; Pei, C.; Gong, J. Propane dehydrogenation: catalyst development, new chemistry, and emerging technologies. *Chem. Soc. Rev.* **2021**, *50* (5), 3315−3354.
(38) Sattler, J. J.; Ruiz-Martinez, J.; Santillan-Jimenez, E.; Weckhuysen, B. M. Catalytic dehydrogenation of light alkanes on metals and metal oxides. *Chem. Rev.* **2014**, *114* (20), 10613−10653.
(39) Zhou, Y.; Thirumalai, H.; Smith, S. K.; Whitmire, K. H.; Liu, J.; Frenkel, A. I.; Grabow, L. C.; Rimer, J. D. Ethylene Dehydroaromatization over Ga-ZSM-5 Catalysts: Nature and Role of Gallium Speciation. *Angew. Chem., Int. Ed. Engl.* **2020**, *59* (44), 19592−19601.
(40) Phadke, N. M.; Van der Mynsbrugge, J.; Mansoor, E.; Getsoian, A. B.; Head-Gordon, M.; Bell, A. T. Characterization of Isolated Ga^{3+} Cations in Ga/H-MFI Prepared by Vapor-Phase Exchange of H-MFI Zeolite with $GaCl_3$. *ACS Catal.* **2018**, *8* (7), 6106−6126.
(41) Xin, M.; Xing, E.; Gao, X.; Wang, Y.; Ouyang, Y.; Xu, G.; Luo, Y.; Shu, X. Ga Substitution during Modification of ZSM-5 and Its Influences on Catalytic Aromatization Performance. *Ind. Eng. Chem. Res.* **2019**, *58* (17), 6970−6981.
(42) Lee, B. J.; Lee, J. H.; Kim, D. H.; Hur, Y. G.; Lee, K.-Y. Synthesis of aluminum and gallium-incorporated MFI zeotypes and their catalytic activity for ethane dehydroaromatization. *Microporous Mesoporous Mater.* **2021**, *323*, No. 111243.
(43) Schreiber, M. W.; Plaisance, C. P.; Baumgartl, M.; Reuter, K.; Jentys, A.; Bermejo-Deval, R.; Lercher, J. A. Lewis-Bronsted Acid Pairs in Ga/H-ZSM-5 To Catalyze Dehydrogenation of Light Alkanes. *J. Am. Chem. Soc.* **2018**, *140* (14), 4849−4859.
(44) Wang, H.; Shiju, N. R. A mini review on aromatization of n-alkanes. *React. Chem. Eng.* **2025**, *10* (4), 768−776.
(45) Bian, M.; Shu, X.; Xiao, X.; Wang, P.; Pang, S.; Zhao, C.; Fan, X.; Kong, L.; Xie, Z.; Zhao, Z. Precision Engineering of Zeolite Catalysts for Light Hydrocarbon Cracking to Light Olefins: Advances and Challenges. *ChemCatChem* **2025**, *17* (23), No. e00952.
(46) Qian, K.; Tian, W.; Yan, S.; Li, W.; Yin, L.; Guo, D.; Yang, Z.; Chen, D.; Feng, Y. Aromatization of HDPE and PP over Ga-promoted zeolite: Effects of pretreatment and zeolite type. *Fuel* **2024**, *357*, No. 129781.
(47) Guo, D.; Zhu, M.; Yang, Z.; Han, Y.-F. Insights into Catalytic Cracking of n-Heptane over Ga-Doped Hierarchical ZSM-5. *Ind. Eng. Chem. Res.* **2024**, *63* (25), 10965−10980.
(48) Phadke, N. M.; Mansoor, E.; Bondil, M.; Head-Gordon, M.; Bell, A. T. Mechanism and Kinetics of Propane Dehydrogenation and Cracking over Ga/H-MFI Prepared via Vapor-Phase Exchange of H-MFI with $GaCl_3$. *J. Am. Chem. Soc.* **2019**, *141* (4), 1614−1627.
(49) Phadke, N. M.; Mansoor, E.; Head-Gordon, M.; Bell, A. T. Mechanism and Kinetics of Light Alkane Dehydrogenation and Cracking over Isolated Ga Species in Ga/H-MFI. *ACS Catal.* **2021**, *11* (4), 2062−2075.
(50) Ni, Z.; Li, Y.; Zhang, Y.; Wang, Y.; Cui, G.; Jiang, G.; Zhao, Z.; Xu, C. Effect of redox atmosphere treatment on bifunctional Ga/ZSM-5 for efficient catalytic cracking of n-butane. *Chem. Eng. Sci.* **2021**, *245*, No. 116856.
(51) Wu, H.; Wang, Y.; Wu, P.; Fan, H.; Liu, Y.; Liu, S.; Bai, P.; Yan, Z.; Mintova, S. Superior performance of Ga-MFI zeolite with a hierarchical structure and moderate acidity in the catalytic cracking of low-density polyethylene. *Inorg. Chem. Front.* **2026**, *13*, 112.
(52) Wang, Y.; Cheng, L.; Gu, J.; Zhang, Y.; Wu, J.; Yuan, H.; Chen, Y. Catalytic Pyrolysis of Polyethylene for the Selective Production of Monocyclic Aromatics over the Zinc-Loaded ZSM-5 Catalyst. *ACS Omega* **2022**, *7* (3), 2752−2765.
(53) Fu, L.; Xiong, Q.; Wang, Q.; Cai, L.; Chen, Z.; Zhou, Y. Catalytic Pyrolysis of Waste Polyethylene Using Combined CaO and Ga/ZSM-5 Catalysts for High Value-Added Aromatics Production. *ACS Sustainable Chem. Eng.* **2022**, *10* (29), 9612−9623.
(54) Shao, C.-T.; Lang, W.-Z.; Yan, X.; Guo, Y.-J. Catalytic performance of gallium oxide based-catalysts for the propane dehydrogenation reaction: effects of support and loading amount. *RSC Adv.* **2017**, *7* (8), 4710−4723.
(55) Geng, R.; Niu, X.; Liu, Y. Effect of extra-framework Ga_2O_3 species in Ga/ZSM-5 catalysts on methanol-to-aromatics reaction. *Microporous Mesoporous Mater.* **2026**, *400*, No. 113907.
(56) Caiola, A.; Robinson, B.; Bai, X.; Shekhawat, D.; Hu, J. Study of the Hydrogen Pretreatment of Gallium and Platinum Promoted ZSM-5 for the Ethane Dehydroaromatization Reaction. *Ind. Eng. Chem. Res.* **2021**, *60* (30), 11421−11431.
(57) Basila, M. R.; Kantner, T. R.; Rhee, K. H. The Nature of the Acidic Sites on a Silica-Alumina Characterization by Infrared Spectroscopic Studies of Trimethylamine and Pyridine Chemisorption1. *J. Phys. Chem.* **2002**, *68* (11), 3197−3207.
(58) Huber, P.; Studt, F.; Plessow, P. N. Reactivity of Surface Lewis and Brønsted Acid Sites in Zeolite Catalysis: A Computational Case Study of DME Synthesis Using H-SSZ-13. *J. Phys. Chem. C* **2022**, *126* (13), 5896−5905.
(59) Xiao, H.; Zhang, J.; Wang, P.; Zhang, Z.; Zhang, Q.; Xie, H.; Yang, G.; Han, Y.; Tan, Y. Mechanistic insight to acidity effects of Ga/HZSM-5 on its activity for propane aromatization. *RSC Adv.* **2015**, *5* (112), 92222−92233.
(60) Getsoian, A. B.; Das, U.; Camacho-Bunquin, J.; Zhang, G.; Gallagher, J. R.; Hu, B.; Cheah, S.; Schaidle, J. A.; Ruddy, D. A.; Hensley, J. E.; Krause, T. R.; Curtiss, L. A.; Miller, J. T.; Hock, A. S. Organometallic model complexes elucidate the active gallium species in alkane dehydrogenation catalysts based on ligand effects in Ga K-edge XANES. *Catal. Sci. Technol.* **2016**, *6* (16), 6339−6353.
(61) Chalmers, J. A.; Vila, F. D.; Li, L.; Hoffman, A. S.; Dong, J.; Bare, S. R.; Scott, S. L. Majority Ga(I) Sites in H_2−Activated Ga/γ-Al_2O_3 and Ga/ZSM5 Catalysts Exhibit Distinctive XANES and Anomalous EXAFS Behavior. *ACS Catal.* **2026**, *16* (3), 2646−2657.
(62) Xiao, H.; Zhang, J.; Wang, X.; Zhang, Q.; Xie, H.; Han, Y.; Tan, Y. A highly efficient Ga/ZSM-5 catalyst prepared by formic acid impregnation and in situ treatment for propane aromatization. *Catal. Sci. Technol.* **2015**, *5* (8), 4081−4090.
(63) Yuan, Y.; Brady, C.; Annamalai, L.; Lobo, R. F.; Xu, B. Ga speciation in Ga/H-ZSM-5 by in-situ transmission FTIR spectroscopy. *J. Catal.* **2021**, *393*, 60−69.
(64) Li, L.; Chalmers, J. A.; Bare, S. R.; Scott, S. L.; Vila, F. D. Rigorous Oxidation State Assignments for Supported Ga-Containing Catalysts Using Theory-Informed X-ray Absorption Spectroscopy Signatures from Well-Defined Ga(I) and Ga(III) Compounds. *ACS Catal.* **2023**, *13* (10), 6549−6561.
(65) Rejman, S.; Reverdy, Z. M.; Bor, Z.; Louwen, J. N.; Rieg, C.; Dorresteijn, J. M.; van der Waal, J. K.; Vogt, E. T. C.; Vollmer, I.; Weckhuysen, B. M. External acidity as performance descriptor in polyolefin cracking using zeolite-based materials. *Nat. Commun.* **2025**, *16* (1), 2980.

Downloaded from pubs.acs.org/acscatal/article-pdf/doi/10.1021/acscatal.6c06722/6897313/cs-2026-067228.pdf?guestAccessKey=2e356292-6312-461c-9958-d129ff7cd027 by MASSACHUSETTS INST OF TECHNOLOGY user on 26 October 2026

https://doi.org/10.1021/acscatal.6c06722
ACS Catal. XXXX, XXX, XXX−XXX

(66) Pennel, M. L.; Maurya, A. K.; Ebrahim, A. M.; Tassone, C. J.; Cargnello, M. Activity of Silica-Alumina for the Conversion of Polyethylene into Tunable Aromatics Below Pyrolytic Temperatures. *ACS Sustainable Chem. Eng.* **2023**, *11* (34), 12623−12630.
(67) Balzer, A. H.; Hinton, Z. R.; Vance, B. C.; Vlachos, D. G.; Korley, L. T. J.; Epps, T. H. III Tracking Chain Populations and Branching Structure during Polyethylene Deconstruction Processes. *ACS Cent. Sci.* **2024**, *10* (9), 1755−1764.
(68) Sandholm, R. M.; Boehlich, G. J.; Dahl, O.; Chowreddy, R. R.; Stepnov, A.; Vaaje-Kolstad, G.; La Rosa, S. L. Microbial degradation of a widely used model polyethylene is restricted to medium- and long-chain alkanes and their oxidized derivatives. *ISME J.* **2025**, *19* (1), No. wraf276.
(69) Cuthbertson, A. A.; Lincoln, C.; Miscall, J.; Stanley, L. M.; Maurya, A. K.; Asundi, A. S.; Tassone, C. J.; Rorrer, N. A.; Beckham, G. T. Characterization of polymer properties and identification of additives in commercially available research plastics. *Green Chem.* **2024**, *26* (12), 7067−7090.

Downloaded from pubs.acs.org/acscatsc/article-pdf/doi/10.1021/acscatal.6c06722/6897313131/cs-2026-067228.pdf?guestAccessKey=2e356292-6312-461c-9958-d129ff7cd027 by MASSACHUSETTS INST OF TECHNOLOGY user on 26 October 2026

https://doi.org/10.1021/acscatal.6c06722
ACS Catal. XXXX, XXX, XXX−XXX